Particulate Science and Technology

ISSN: 0272-6351 (Print) 1548-0046 (Online) Journal homepage: http://www.tandfonline.com/loi/upst20

# An Experimental and Numerical Study of Transversal Dispersion of Granular Material on a Vibrating Conveyor

**Erdem Simsek , Siegmar Wirtz , Viktor Scherer , Harald Kruggel-Emden , Rafal Grochowski & Peter Walzel**

**To cite this article:** Erdem Simsek , Siegmar Wirtz , Viktor Scherer , Harald Kruggel-Emden , Rafal Grochowski & Peter Walzel (2008) An Experimental and Numerical Study of Transversal Dispersion of Granular Material on a Vibrating Conveyor, Particulate Science and Technology, 26:2, 177-196, DOI: 10.1080/02726350801903772

**To link to this article:** https://doi.org/10.1080/02726350801903772

*Particulate Science and Technology*, 26: 177–196, 2008

ISSN: 0272-6351 print/1548-0046 online
DOI: 10.1080/02726350801903772

Taylor & Francis
Taylor & Francis Group

# An Experimental and Numerical Study of Transversal Dispersion of Granular Material on a Vibrating Conveyor

ERDEM SIMSEK[1], SIEGMAR WIRTZ[1], VIKTOR SCHERER[1], HARALD KRUGGEL-EMDEN[1], RAFAL GROCHOWSKI[2], AND PETER WALZEL[2]

[1]Department of Energy Plant Technology (LEAT), Ruhr-Universitaet Bochum, Bochum, Germany
[2]Department of Biochemical and Chemical Engineering, University of Dortmund, Dortmund, Germany

*The mixing of thin granular layers transported on the surface of an oscillating trough is experimentally and numerically examined. The particle dispersion was experimentally quantified by an image processing system recording the growth of the mixing layer thickness of two differently colored but otherwise identical sand particle streams along the longitudinal position within the transporting channel. Granular flow and dispersion on the vibrating conveyor were studied numerically based on a three-dimensional discrete element code. Both experiments and simulations were used to derive quantities characterizing the transversal dispersion. The mixing was found to be directly proportional to the vertical acceleration of the conveyor and inversely proportional to the mass flow of the transported material. Keeping the above-mentioned parameters constant, the dispersion increases with increasing mean particle diameter. When performing the experiments with materials of different mean particle diameters and tuning the mass flow to achieve the same level of dimensionless bed height, the magnitude of the dispersion coefficient remains constant, as was also confirmed by the numerical simulation.*

**Keywords** diffusion, discrete element simulation, dispersion, granular material, image processing, mixing, vibration

## Introduction

Despite frequent use and many industrial applications, the design of vibrating machines is still mostly based on practical experience. The goal of this cooperative project was to experimentally examine the mechanisms of transport and behavior of granular material in a vibrating conveyor and confirm the results with a discrete element simulation. A prototype apparatus was designed to perform experiments within a large range of adjustable parameters. After a detailed investigation of the transport properties of coarse sand layers submitted to linear, circular, and elliptic modes of vibration (Grochowski et al., 2004a,b), the next step of the study was

Address correspondence to Erdem Simsek, Department of Energy Plant Technology (LEAT), Ruhr-Universitaet Bochum, Universitaetsstraße 150, D-44780, Bochum, Germany. E-mail: simsek@leat.rub.de

the examination of mixing effects occurring within the bed. A preliminary report of the first experimental results on this subject may be found in Grochowski and Walzel (2005). The discrete element code developed at the Department of Energy Plant Technology (LEAT), Ruhr-Universität Bochum, showed satisfactory results in simulating the behavior of granular materials on conveying equipment (Kruggel-Emden et al., 2007) and in staged reforming processes for biomass and waste utilization that employ a solid heat carrier (Kruggel-Emden et al., 2006a; Ivanov et al., 2004).

Mixing of solids is recognized as an important unit operation in process engineering (Weinekötter & Gericke). Independent of the kind of device, mixing occurs due to two fundamental mechanisms: (i) convective motion of particle lumps and (ii) individual particle displacement, i.e., dispersion (Sommer, 1977). Most examinations concerning mixing in vibrating beds were performed in closed, vertical, and usually two-dimensional convection-dominated systems (Hunt et al., 1994; Hsiau et al., 2002; Ko, 2005; Lu & Hsiau, 2005, Submitted; Tai & Hsiau, 2004; Akiyama & Nishiyama, 1994; Akiyama et al., 1998). Results of those studies may unfortunately not be directly applicable to an open input-output system like a vibrating conveyor. To start their analysis the authors decided to focus on the dispersion mechanism. Thus, the subject of investigation is a particular property of the bed: the transversal dispersion occurring in thin layers in a steady-state flow. Several experimental investigations on the topic of diffusion-based mixing were performed in shear granular flows, in horizontally oriented devices (Buggisch & Löffelmann, 1989; Hsiau et al., 2005; Scott & Bridgewater, 1976) or in vertical channels (Hsiau & Hunt, 1993; Natarajan et al., 1995). Dispersion of a strip of colored beads in a two-dimensional vertically vibrated bed was studied by Zik and Stavans (1991). In the references mentioned, the authors could fit the concentration distribution to the diffusion equation, concluding the diffusive nature of the process.

The current study uses a three-dimensional soft particle discrete element method (DEM) to simulate the behavior of particles in a vibrated granular bed. DEM is able to give detailed information on events and conditions within the bed, including contact forces and velocities. The discrete element method was first used to simulate granular flow by Cundall and Strack (1979), and since then it has been applied to various simulation models in several fields, including granular mixing in vibrated beds (Lu & Hsiau, 2005, Submitted; Campbell, 1997; Cleary et al., 1998; Henrique et al., 2000; Asmar et al., 2002; Rhodes et al., 2001; Hsiau & Yang, 2003; Ivanov et al., 2004).

However, both experimental and theoretical studies use idealized systems, for example, two-dimensional geometries or bulks consisting of glass beads, whose regular shape and low friction do not necessarily correspond to real solid systems encountered in industrial practice. Nevertheless, in the present work the authors intend to use the dense-gas kinetic theory approach (Campbell, 1990; Jenkins & Savage, 1983; Ogawa, 1978) to investigate the mixing behavior in a "real" granular flow, i.e., coarse natural sand with irregular shape and poly-distributed particle size. The subject of discussion will be the correctness of implementation of particular parameters of the equation describing the mixing kinetics. The analysis of the mixing process may lead to a better explanation of transport mechanisms in the conveyor, for example, to understand the principle of transition between the bulk and single-particle movement regime. Additionally, the results will be used to validate the simulation technique mentioned in the beginning.

## Experimental Setup and Procedure

The experimental facility is shown in Figure 1. Two streams of differently colored but otherwise identical granular materials were charged to the setup, each with a given mass flow $\dot{m}_{in}$ with two volumetric feeders (Brabender-Flex Wall Plus FW40). The sand streams were then separately transported in an equalizing conveyor (AEG Vibrationstechnik, KP 6-1) and loaded in parallel onto the surface of the experimental trough. In order to avoid spontaneous mixing during the feeding at the trough's inlet, a thin splitting plastic sheet was fixed to its surface along the transport axis. Once the streams join at the sheet edge, they create a uniform layer on the surface of the channel. The bulk was then conveyed and discharged through a two-way output funnel into a box placed on a digital balance (Sartorius LC12000). A PC read out the discrete measurement of the balance $m(t)$ at four-second intervals. The mass flow $\dot{m}_{out}$ leaving the trough was determined by subtracting the last read out from the previously acquired one. Fluctuations of the readout signal due to pulsation of the feeders were less then 8%. A flap driven by a servomotor, wired with the drive of the equalizing conveyor, served to direct the material to one or the other output of the funnel.

After steady-state conditions $\dot{m}_{out} = \dot{m}_{in}$ were obtained, the flap was switched; at the same time the equalizing conveyor stopped to load the material to the trough. Thus the holdup $m_h$, i.e., the material present on the conveying channel in the stationary process, could be collected in a separate box. With the length $L$ of the trough the mean transport velocity was calculated as:

$$\bar{u} = \frac{L \cdot \dot{m}_{out}}{m_h} \tag{1}$$

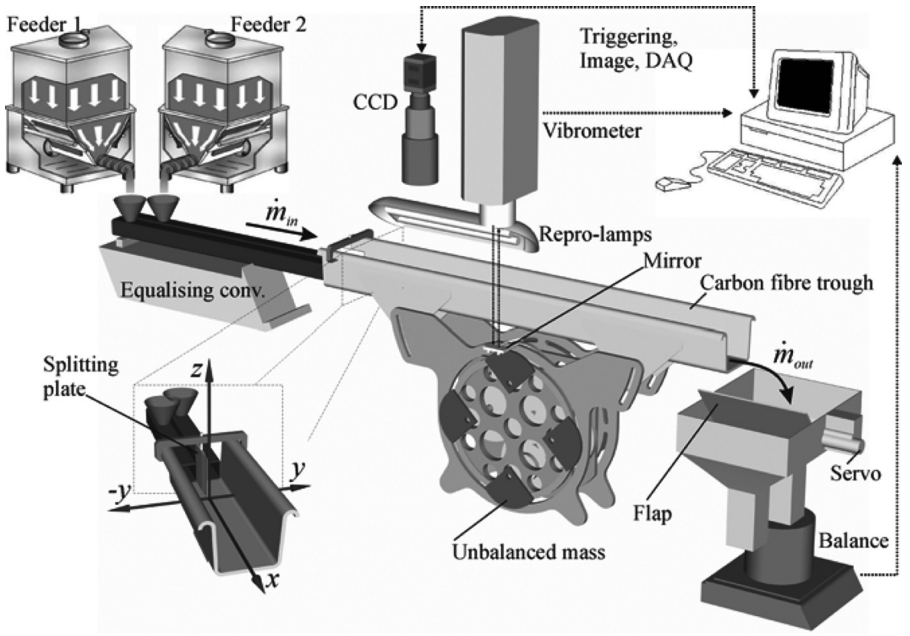


**Figure 1.** Experimental setup of conveying system; coordinate origin is placed at the edge of the splitting plate.

**Table 1.** Parameters of the vibrating conveyor; all experimental results in this study are measured with linear vibration mode and a horizontal channel $\beta = 0^\circ$

| Parameter | Value |
|---|---|
| Trough | Material: composite carbon fiber and epoxy resin Wall thickness: 3 mm; $B = 70$ mm; $L = 800$ mm |
| Oscillation modes | Linear, elliptic, circular (linear used here) |
| Vibration angle | $0^\circ < \alpha < 90^\circ$ |
| Inclination angle | $+8^\circ < \beta < -8^\circ$ ($\beta = 0^\circ$ used here) |
| Vibration frequency | $\omega = 2\pi$f, frequency $0 <$ f $< 100$ Hz |
| Amplitude | $A = 2$; 3; 4; 5 mm |
| Acceleration coefficient | $K_V = 0 \ldots 10$ [ − ] |

The theoretical bed height, or in other words the thickness of the "condensed" layer, was determined from:

$$h = \frac{m_h}{B \cdot L \cdot \rho_b} \tag{2}$$

where $B$ is the width of the trough and $\rho_b$ is the material bulk density. The construction of the conveyor enables rotation of the driving unit and thus the adjustment of the vibration angle α. A laser vibrometer (Polytec OFV 302 Sensor Head) continuously read the frequency $f$ as well as the vertical displacement $A_V$ of the machine, while the oscillation amplitude was derived from $A = A_V/\sin\alpha$. A major parameter characterizing the adjustment of a vibrating conveyor is the dimensionless acceleration coefficient $K_V = A \cdot sin\,\alpha \cdot (2\pi f)^2/g$, where $g$ is the gravitational acceleration. Dimensions and possible settings are listed in Table 1. A more detailed description of the working principle and the design of the apparatus may be found in Grochowski et al. (2004a,b).

Natural quartz sand or quartz gravels (Siligran, Euroquarz GmbH, Germany) were used as granular material for the experiments. The same particles only coated by black epoxy resin (Colorquarz No. 911) were used as a second component for the mixing tests. In order to investigate the influence of the particle diameter $d_p$ the material was sieved in adequate size fractions. The size distribution is presented in Table 2.

**Table 2.** Particle size distributions of the sand fractions; $d_{05,3}$ and $d_{95,3}$ are the lower and upper limits between which 90% of the mass of the size fractions are distributed

| | Black sand (B) | | | Natural sand (W) | | | |
|---|---|---|---|---|---|---|---|
| Color fraction | $d_{05,3}$ [mm] | $\bar{d}_p$ [mm] | $d_{95,3}$ [mm] | $d_{05,3}$ [mm] | $\bar{d}_p$ [mm] | $d_{95,3}$ [mm] | Mean particle diameter $\bar{d}_p$ [mm] |
| Small | 0.71 | 0.87 | 1.00 | 0.79 | 0.96 | 1.12 | **0.92** |
| Medium | 1.23 | 1.39 | 1.55 | 1.25 | 1.42 | 1.56 | **1.41** |
| Large | 1.50 | 1.77 | 1.98 | 1.46 | 1.73 | 1.87 | **1.75** |

In order to compare measurements carried out with different size fractions and mass flows, the dimensionless bed height $h^* = h/\bar{d}_p$ is introduced, representing the number of particle layers "at rest" of the bulk.

Investigations of the particle dispersion behavior involved the visual observation of the top surface layer of the particle flow. A black and white CCD-camera (PixelFly, PCO) was placed on the top of the trough, recording the mixing process of the two granular streams. In order to ensure a uniformly distributed illumination and to minimize reflections from the surface of single particles, special cold diffusive lighting units were used (Kaiser Fototechnik, RB 218).

Since the trough displaces vertically during the operation, it was necessary to record each consecutive image in a series of measurements in the same position, i.e., in the same phase of the oscillation. For this purpose, the camera was externally triggered with use of a transistor–transistor logic (TTL) signal generated by a data acquisition (DAQ) card (NI-6601). The start of the triggering signal was released manually, i.e., randomly. This means that the series of images in individual experiments were recorded in different phases of motion. Additional tests comparing the evaluation of the experimental data acquired for the same settings of the conveyor proved that the influence of the phase on the results (concentration field) could be neglected. Thus, it was not necessary to control this parameter (start of the trigger signal depending on the phase of oscillation). Depending on the velocity of the moving bulk, the pictures were acquired with $f/k$ frames per second ratio, where $k$ is an integer $k = 6, 7, 8$ and $f$ is the frequency of the conveyor oscillation. For each experiment a series of $n = 256$ pictures were recorded (all in the same phase, see above). The images were processed with Image-Pro Plus software (Media Cybernetics). Their original size was cropped to an $i \times j = 1200 \times 200$ pixel region, with optical resolution ranging from $\sim$4.5 to $\sim$5.5 pixel/mm. This corresponds to 26 cm of the trough length and 4.3 cm of its width, symmetrically enclosing both particle streams (see Figure 2(a)). The cropping window was shifted in the picture in order to show at the left side the edge of the separating plate used to set the coordinate origin.

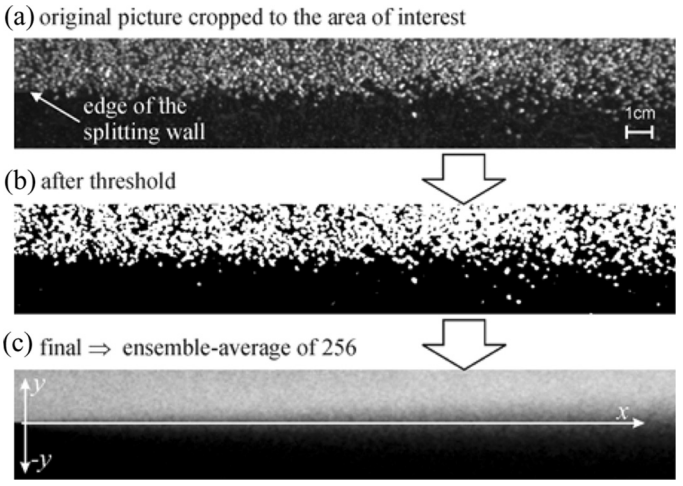


**Figure 2.** Scheme of image processing; 256 pictures were taken for each experiment. Images presented on the scheme correspond to following process parameters: $A = 2.2$ mm, $\alpha = 22^\circ$, $K_V = 2$, $\bar{d}_p = 1.41$ mm, $\dot{m}_{in} = 60$ Kg/h. Evaluation of this measurement is shown in Figure 10.

A segmentation function was applied to extract objects, i.e., grains, by locating pixels of the specified gray level and setting everything else to black. Thus, the brighter (natural sand) particles were identified (Figure 2(b)), and the image was saved in a binary format where the pixels may obtain either 0 or 1 value (0 means black, 1 means white). The range value, above which particular pixels of the original image were treated as belonging to a natural sand particle (threshold value), was readjusted for each series of experiments depending on the overall brightness of the pictures.

In the next step, an ensemble-average image was calculated from 256 binary pictures processed in the previous step. Values of particular pixel positions $[i, j]$ of all $n$ images were summed and divided by the total number of $n = 256$ operands. The resulting matrix was a time-averaged local concentration distribution of the brighter particles transported on the channel during the experiment. Its graphic representation, scaled by 256, is shown on a gray scale image in Figure 2(c).

Then, the concentration field of white fraction $C_w$ was determined. The result was loaded in the form of a two-dimensional matrix into mathematical software (Mathcad, Mathsoft). In order to smooth the experimental data, the resolution of the $C_w$ field was decreased by a factor of 25. The value of each element was recalculated as the average of $5 \times 5$ pixels of the original matrix. As shown in Figure 3, the local concentration distribution depending on the transversal position $y$ follows an S-shaped curve. It is characterized by a sharp gradient at the inlet position and flattens out with increasing transport length.

At each x position a sigmoid function was approximated laterally to the distribution field:

$$C_w(y) = c_0 + \frac{a}{1 + e^{-\frac{y - y_0}{b}}}$$

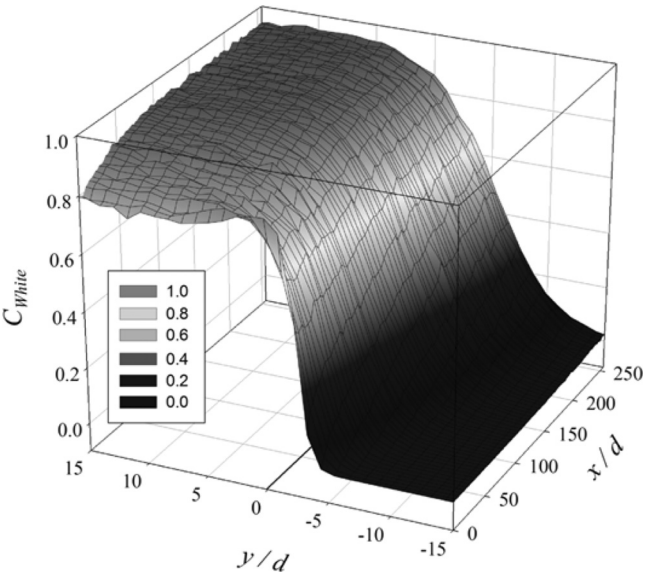


**Figure 3.** Averaged concentration distribution against the position on the picture.

where $a$, $b$, $c_0$, and $y_0$ are the fitted parameters. By solving the fitting function, e.g., for $C_w = 0.05$, enabled identifying the course of the mixing layer thickness $\delta$ (defined as the transversal distance over which the concentration varies from 5% to 95%). Since preliminary tests showed that the concentration distribution was symmetrical for both fractions, further analysis was performed only for the ''white fraction.'' For each experiment a calibration picture was taken, the position in the concentration distribution matrix being rescaled to the trough coordinate system (origin at the edge of the separating plate; see Figure 1).

## Discrete Element Simulation

The discrete element method provides a way of describing particle systems by modeling each particle and its interactions with its surrounding individually over time (Lätzel et al., 2003; Goda & Ebert, 2005; Langston et al., 2004). Thus, the motion of a particle is computed by calculating all forces acting on it while integrating the equations of motion numerically.

Newton's and Euler's equations

$$m_i \frac{d^2\vec{x}_i}{dt^2} = \sum_{j=1}^{N} \vec{F}_{ij} + m_i\vec{g} \tag{3}$$

$$J_i \frac{d^2\vec{\varphi}_i}{dt^2} = \sum_{j=1}^{N} \vec{M}_{ij} \tag{4}$$

with mass $m$, moment of inertia $J$, acceleration $d^2\vec{x}_i/dt^2$, angular acceleration $d^2\vec{\varphi}_i/dt^2$, and external moments $\vec{M}$ describe the translational and rotational motion. For the force balance within the equations of motion the contact forces can be decomposed in their normal and tangential components. Gravitational forces must be accounted for, and external moments that affect rotational motion are caused by tangential forces. When all forces are determined, the equations of motion must be integrated numerically. For this purpose several integration schemes are applicable (Rougier et al., 2004). Because of their simplicity and the low computational effort required, single-step explicit schemes with constant time steps are most frequently used.

Due to the objective of simulating large particle assemblies with the discrete element method, as is essential for industrial applications, there is the need to model the contact forces by fast approaches. Therefore the particles in a discrete element model generally are assumed rigid but they are allowed to overlap in order to model their deformation during collision. This overlap $\delta$ for spherical particles, which is given by:

$$\delta = \frac{1}{2}(d_i + d_j) - (\vec{x}_i - \vec{x}_j) \cdot \vec{n} \tag{5}$$

is used to determine contact forces of the bodies, where $d_i$, $d_j$ are the particle diameters and $\vec{x}_i$, $\vec{x}_j$ are the positions of the particle centers, with the normal vector $\vec{n}$ pointing from the center of particle $j$ to $i$. The normal velocity of the contact point of particle $i$ while overlapping particle $j$ can be derived from the particle velocities $\vec{v}_i$

and $\vec{v}_j$ as

$$\vec{v}^n = -((\vec{v}_i - \vec{v}_j) \cdot \vec{n})\vec{n} \tag{6}$$

The normal force during contact of two particles or a particle and a wall can be modeled by a simple approach based on the overlap and the normal velocity. The equation is identical to the equation of a linear harmonic damper consisting of an elastic repulsive force combined with a dissipative component:

$$\vec{F}^n = \vec{F}^n_{el} + \vec{F}^n_{diss} = k^n \delta \vec{n} + \gamma^n \vec{v}^n \tag{7}$$

where $k^n$ is the stiffness of a linear spring and $\gamma^n$ is a damping coefficient. A force model like (7) leads to a constant coefficient of normal restitution and a constant collision time being independent of the initial normal velocity $\vec{v}^n_0$. However, experiments indicate that both collision properties decrease with increasing initial normal velocity (Schäfer et al., 1996; Kruggel-Emden et al., 2006b, In press), making the aforementioned statement unphysical. Nevertheless, in cases where the velocities vary not too strongly, like in the situation of a packed bed, a force law like (7) may still be suitable. Both coefficients $k^n$ and $\gamma^n$ are of empirical nature and need to be calibrated to averaged data for the coefficient of restitution and the mean collision time.

In the tangential direction the tangential velocity of a particle's contact point can be obtained from the relative velocity at this point by

$$\vec{v}^t = \vec{v}_{ij} - (\vec{v}_{ij} \cdot \vec{n})\vec{n} \tag{8}$$

with the relative velocity given as

$$\vec{v}_{ij} = (\vec{v}_i - \vec{v}_j) - \frac{1}{2}(\vec{\omega}_i d_i + \vec{\omega}_j d_j) \times \vec{n} \tag{9}$$

where $\vec{\omega}_i$, $\vec{\omega}_j$ are the angular velocities of the particles in a collision. Similar to the normal unit vector $\vec{n}$, a tangential unit vector $\vec{t} = \vec{v}^t/|\vec{v}^t|$ can be derived from the tangential velocity.

For the contact point a tangential coordinate $\xi$ can be introduced expressing the relative tangential displacement of the two points of the colliding bodies being primarily in contact. At the initiation of the collision $\xi$ is zero, being then integrated over the entire contact duration:

$$\xi = \left( \int_{t_0}^{t_f} \vec{v}^t(t')dt' \right) \cdot \vec{t} \tag{10}$$

A tangential contact force can be stated as

$$\vec{F}^t = \min(\vec{F}^t_{st}, \vec{F}^t_C) = -\min(k^t \xi, \mu_C |\vec{F}^n|)\vec{\xi}/|\vec{\xi}| \tag{11}$$

where $k^t$ is the stiffness of a linear spring and $\mu_C$ is the Coulomb friction coefficient. A model like (11) was first introduced by Cundall and Strack (1979), which can be understood as a linear spring limited by the Coulomb friction condition. During the contact of two bodies a spring is assigned between both of them, which is then stretched or shortened while the particles stay in contact. A tangential force model like (11) allows particles to reverse their tangential velocity during contact, which

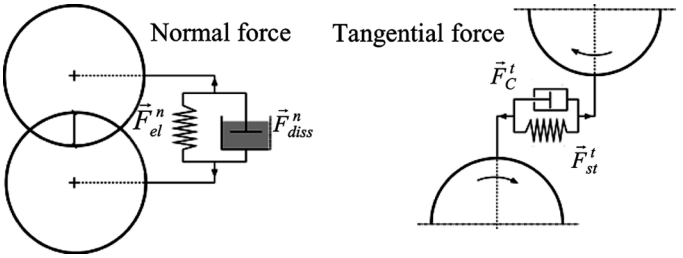


**Figure 4.** Schematic of force models.

is also evident from experiments (Kharaz et al., 2001; Foerster et al., 1994). Even detailed collision properties can be modeled with adequate accuracy (Di Maio & Di Renzo, 2004).

The tangential stiffness $k^t$ can be derived analogous to the elastic case studied by Maw et al. (1976) even in case of a viscoelastic material by

$$k^t = \kappa m \frac{\pi^2}{(t^n)^2} \tag{12}$$

where $\kappa$ is the tangential-to-normal stiffness ratio and $t^n$ is the contact duration. The stiffness ratio is a parameter strongly influencing the performance of a model like (11). It can be obtained from the mechanical properties of the bodies involved in the collision

$$\kappa = \frac{\frac{1-\nu_i}{G_i} + \frac{1-\nu_j}{G_j}}{\frac{1-0.5\nu_i}{G_i} + \frac{1-0.5\nu_j}{G_j}} \tag{13}$$

with $\nu$ being the Poisson ratio and $G$ the shear modulus of the two involved bodies $i$ and $j$.

A graphical representation of the force laws is shown in Figure 4.

## Numerical Setup and Procedure

For the simulations the granular material is assumed to consist of spherical sand particles. The required mechanical properties are summarized in Table 3. The particle size distribution shown in Table 2 is represented by five distinct classes. The dynamic

**Table 3.** Particle properties

| Property | Notation | Value |
|---|---|---|
| Young's modulus [GPa] | E | 2.5 |
| Shear modulus [GPa] | G | 1.02 |
| Particle density [kg/m$^3$] | $\rho$ | 2650 |
| Normal coefficient of restitution | $e^n$ | 0.3 |
| Particle/particle friction coefficient | $\mu_{C,PP}$ | 0.5 |
| Particle/wall friction coefficient | $\mu_{C,PW}$ | 0.5 |

**Table 4.** Material parameters of the model for particle/particle (P/P) and particle/wall (P/W) interaction

| | Property | Notation | Value |
|---|---|---|---|
| | | P/P | P/W |
| Normal spring constant [N/m] | $k^n$ | 1000 | 1000 |
| Normal damping constant [kg/s] | $\gamma^n$ | 0.01–0.017 | 0.030–0.035 |
| Normal-to-tangential spring ratio | $\kappa$ | 0.86 | 0.86 |
| Tangential spring constant [N/m] | $k^t$ | 860 | 860 |

properties describing the interactions between particles and the interaction of particles with walls are chosen as constant. The coefficient of normal restitution and the friction coefficients are selected as listed in Table 3.

The dynamic interaction properties are implemented with the force models described above. The linear stiffness in the normal direction is fixed with $k^n = 1000\,N/m$. The normal damping constant $\gamma^n$ is calculated to match the normal coefficient of restitution of $e^n = 0.3$ both for particle/particle and particle/wall contacts. The normal-to-tangential spring ratio $\kappa$ is calculated according to Di Maio and Di Renzo (2004). Based on this ratio the related tangential stiffness can be calculated with Equation (12). The values of the material interaction parameters are summarized in Table 4.

The walls of the vibrating conveyor are modeled as triangulated surfaces that may move in space over time. The geometry is based on the experimental setup and presented in Figure 5.

The three-dimensional calculations were carried out on a cluster consisting of 14 Alpha XP1000 (EV67) computers. The discrete element simulations were performed with a parallelized particle code recently developed at LEAT. The time span of the simulations covers the range $t = 0$–$40$ s. The selected step size was $\Delta t = 4.85 \times 10^{-6}\,s$. For the initialization of a simulation the vibrating conveyor was loaded with particles on the whole length; the particles were colored either black or white depending on their position. Then the particles were transported by the vibration of the conveyor. Within the simulation all motion modes of the experiments (Table 1) can be realized.

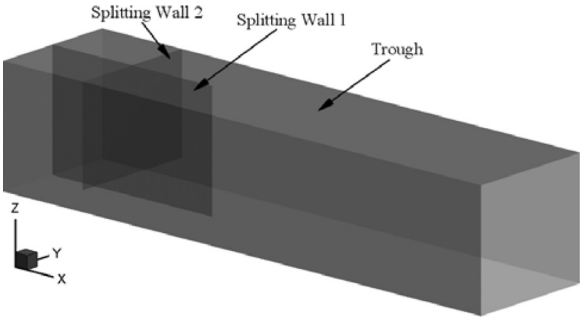


**Figure 5.** Geometry of the vibrating conveyor.

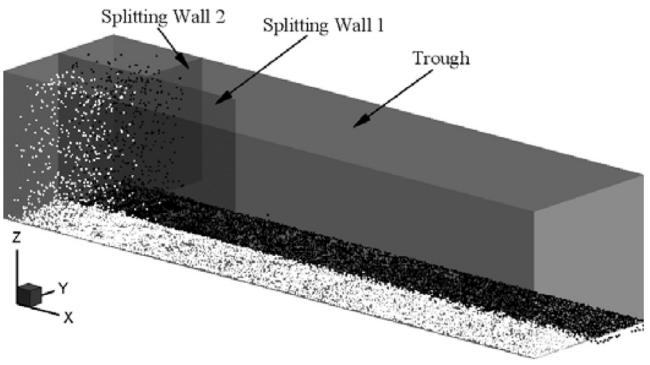


**Figure 6.** Snapshot of the simulation.

All particles that leave the end of the conveyor are detected in order to determine the mass flow rate $\dot{m}_{out}$. The particles at the inlet upstream of splitting wall 2 were introduced with the same mass flow rate $\dot{m}_{in} = \dot{m}_{out}$. The first splitting wall separates the differently colored layers from each other, exactly as in the experiment avoiding dispersion at the inlet of the conveyor. The second splitting wall prevents the particles from uncontrolled entering of the measurement area. A snapshot of the simulation is shown in Figure 6.

Since the position of every particle is known over time in discrete element simulations, the mass on the conveyor at a certain moment, i.e., the holdup $m_h$, can be determined as the sum of all particle masses. The transport velocity, which is important for the analysis of the dispersion, can be computed through Equations (1), and (2) provides the theoretical bed height.

Although the steady-state condition with respect to the incoming and outgoing mass flows is immediately obtained, the vibrating conveyor is operated for some time (10 s) before examination of the dispersion. This approach is necessary to allow the dispersion to fully develop along the vibrating conveyor. For the examination of the dispersion a length of 20 cm beginning from the edge of splitting wall 1 and a time interval of 30 s is considered. A snapshot of the considered range of the vibrating conveyor is shown in Figure 7. This is a top view of a simulation with a dimensionless bed height of $h^* = 0.5$, hence the surface of the trough is not fully covered by the particles.

In order to determine the concentration field $Cw(x, y)$ of the black particles, all particles have to be considered along their path on the conveyor. Therefore, the

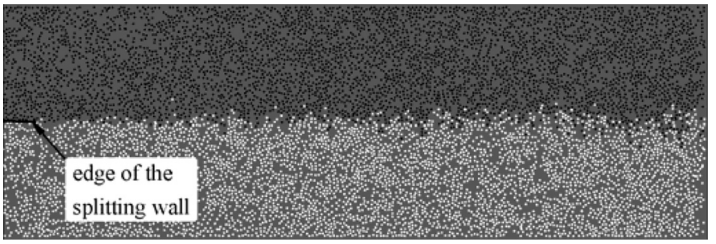


**Figure 7.** Snapshot of the range used for the evaluation.

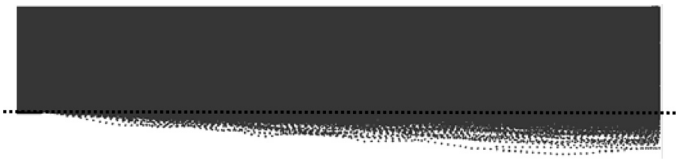

**Figure 8.** Positions of the black particles during the simulation time.

particle positions are recorded each 0.01 s and used in the evaluation. The arising situation is depicted in Figure 8, where the locations of only the black particles are shown.

The development of the mixing zone during the progress of the simulation is visible. The determination of the concentration of the black particles, i.e., the ratio of their volume ($V_{black}$) to the whole particle volume ($V_{black} + V_{white}$), for every position on the conveyor provides the concentration field $C_w(x, y)$ (Figure 3). Analogous to the evaluation of the experiments the concentration field $C_w(x, y)$ for a given value $C_w = 0.05$ can be extracted.

## Results and Discussions

The mixing kinetics can be quantified by means of dispersion coefficients $D_i$. The orientation of the mixing direction is indicated by the subscripts $x$, $y$, and $z$ as shown in Figure 1. The determination of the coefficient is based on a simple analysis of the diffusion equation for a mixing layer. Assuming that the particle's flow velocity $u$ and the dispersion coefficient are constant within the mixing region, the diffusion equation may be rewritten in the following form:

$$\bar{u}\frac{\partial C}{\partial x} = D_y \frac{\partial^2 C}{\partial y^2} \tag{14}$$

The further reasoning is analogous to the procedure described in Hsiau and Hunt (1993). Integration of Equation (14) yields the following concentration distribution:

$$C_w(x, y) = \frac{1}{2} \pm \frac{1}{2} erf\left(\frac{\pm y}{2(x \cdot \bar{d}_p)^{\frac{1}{2}}} Pe^{\frac{1}{2}}\right) \tag{15}$$

where $+$ is for $y > 0$, $-$ for $y < 0$, and $erf(\,)$ is the error function. $Pe$ is the Peclet number defined as the ratio of convective motion to dispersion:

$$Pe = \frac{\bar{u} \cdot \bar{d}_p}{D_y} \tag{16}$$

Solving Equation (15) for $C_w = 0.05$ we obtain the dimensionless mixing layer thickness:

$$\frac{\delta}{\bar{d}_p} = 2.33\sqrt{\frac{x}{\bar{d}_p \cdot Pe}} \tag{17}$$

For each experiment Equation (17) is fit with the least-squares technique to the results. The adapted $Pe$ number is entered into Equation (16), enabling determination of the dispersion coefficient $D_y$.

In order to qualify the influence of individual parameters on the process, several tests were performed. Figure 9 presents the dependence of the mixing process on the acceleration parameter $K_V$. As expected, the dispersion strongly increases as a function of the vibration intensity. For $K_V < 1.5$ practically no mixing was observed, although good transport conditions were already achieved. Measurements for even higher $K_V > 3.3$ would be of further interest in order to check whether the dispersion achieves a maximum value as is observed for the transport velocity (Grochowski et al., 2004a). Interpretation of the data would be more complicated, since for these settings of the oscillation parameters wave formation begins to occur within the granular bed.

The next experiment was run with constant load and constant settings of vibration parameters but different size fractions of conveyed material. Figure 10 clearly shows that the dispersion increases proportionally to the mean particle diameter of the conveyed fraction. It should be noted that when keeping the magnitude of the mass flow $\dot{m}_{in}$ constant with increasing $\bar{d}_p$ the number of particles per unit time decreases with the power of $-3$. All fractions have the same mean transport velocity $\bar{u} = 0.183\,\mathrm{m/s}$ with a deviation $< 5\%$.

The following dispersion coefficients were fit to the data in this experiment: $D_y = 0.88 \times 10^{-6}\,\mathrm{m^2/s}$, $D_y = 9.90 \times 10^{-6}\,\mathrm{m^2/s}$, and $D_y = 21.2 \times 10^{-6}\,\mathrm{m^2/s}$ for "small," "medium," and "large" fraction respectively.

Another effect was observed when the particle diameter was kept constant and the mass flow was varied. Figure 11 shows a reduction of the dispersion with increasing load. Here again a dependence is observed between the amount of particles and the dispersion intensity.

The measured transport velocity increased as a function of rising mass flow during the experiments. Results of other experiments performed by the authors (not yet published) showed that this tendency is valid especially for small mass flows and decays for higher mass flows $\dot{m}_{in} > 60\,\mathrm{kg/h}$.

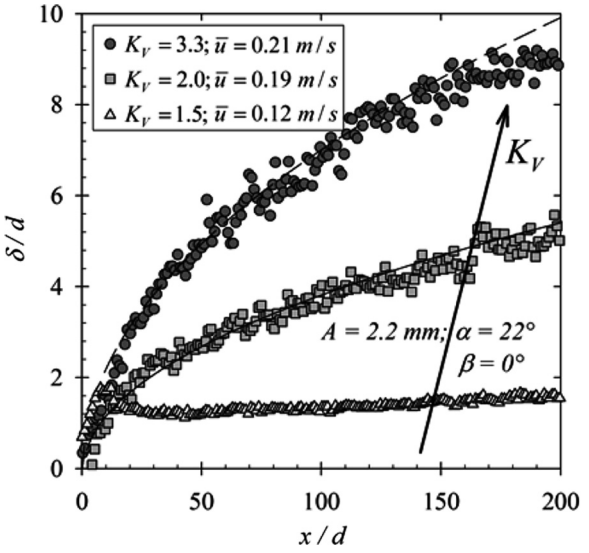


**Figure 9.** Growth of the mixing layer with increasing longitudinal position for different values of $K_V$. Linear vibration, constant mass flow $\dot{m}_{in} = 40\,\mathrm{kg/h}$, particles: "small," $\bar{d}_p = 0.92\,\mathrm{mm}$.

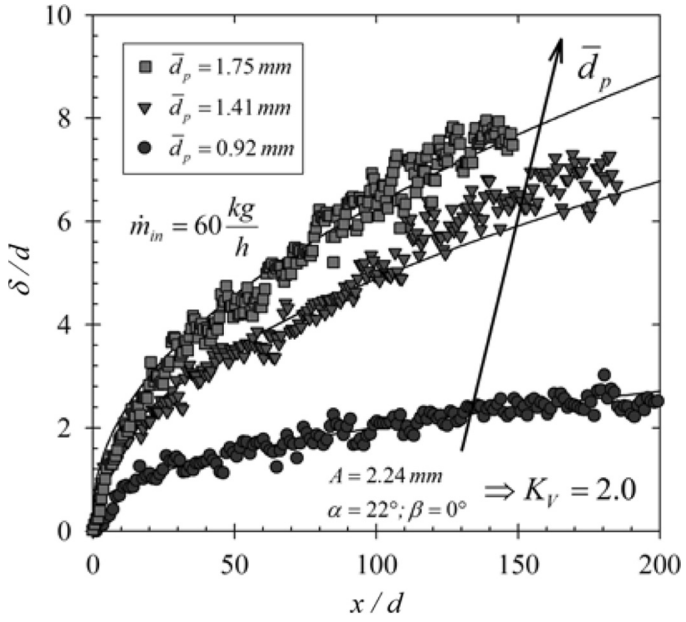


**Figure 10.** Dependence of the mixing layer thickness on the mean particle diameter $\bar{d}_p$ for constant mass flow $\dot{m}_{in}$ and $K_V$.

The authors were in doubt whether the particle diameter was correctly used in the equation describing the mixing kinetic as the scaling parameter of the process. It was found that when running the experiments with different size fractions and

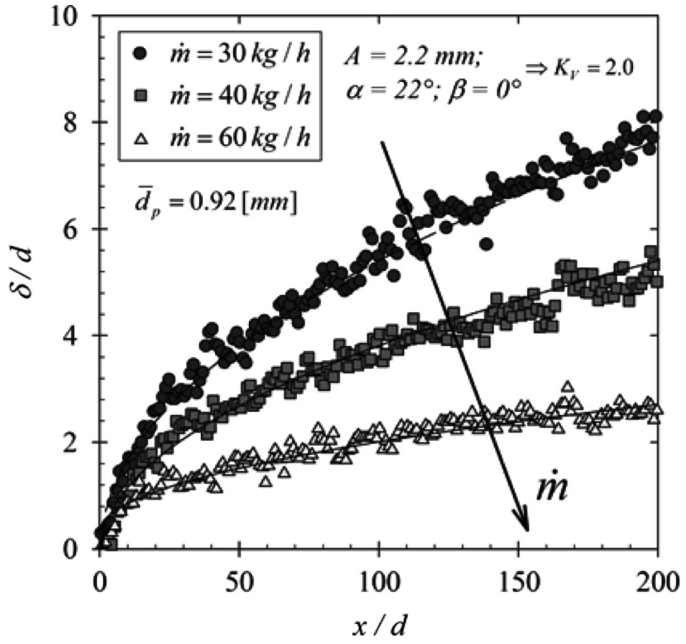


**Figure 11.** Dependence of the mixing layer thickness on the mass flow of material.

tuning the mass flow in order to achieve the same level of dimensionless bed height $h^*$, the points representing the growth of the mixing layer thickness collapsed onto the same curve. Figures 12 and 13 show the results of experiments for the same adjustment of vibration and the same three size fractions of conveyed material but two different levels of the dimensionless bed height, $h^* = 0.5$ and $h^* = 1$ respectively. The mixing was found to be distinctly dependent on $h^*$. Increasing $h^* > 1$ (trough fully covered by particles) strongly reduced the dispersion phenomenon; see Figure 12. However, the dependence of the mean transport velocity on the mass flow and on the particle diameter of conveyed material showed more complex behavior in these two experiments. In case of a very thin layer $h^* = 0.5$ the velocity increased with the particle diameter. For the case of $h^* = 1.0$ (surface of the non-moving trough fully covered by the particles) the velocity remained rather constant, independent of the fraction and transported mass flow. Table 5 lists the dispersion coefficients fitted to each series of data in the experiments. Despite the fact that the mixing layer thickness had exactly the same growth ratio for all fractions, the determined dispersion $D_y$ attained different values. This deviation is caused by the differences in the mean transport velocity achieved at steady state. However, the ratio of the velocity to the dispersion coefficient remained constant when scaled by the particle diameter, which is the Peclet number according to Equation (16).

The same experiments were repeated for two additional amplitudes with an oscillation of 0.89 mm and 4.22 mm, showing behavior analogous to that of the mixing.

For the numerical simulation, cases with different size fractions but a constant dimensionless layer thickness $h^*$ (Figures 12 and 13) were selected, because in these cases many complex physical effects lead to a constant growth of the mixing layer thickness. Therefore, these experiments are suited for validation purposes of the

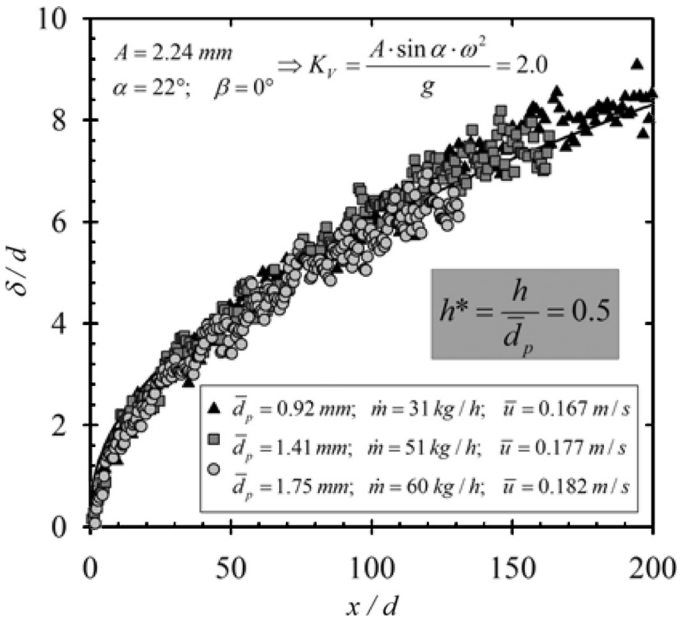


**Figure 12.** Growth of the mixing layer thickness for different size fractions and constant dimensionless bed height $h^* = 0.5$.

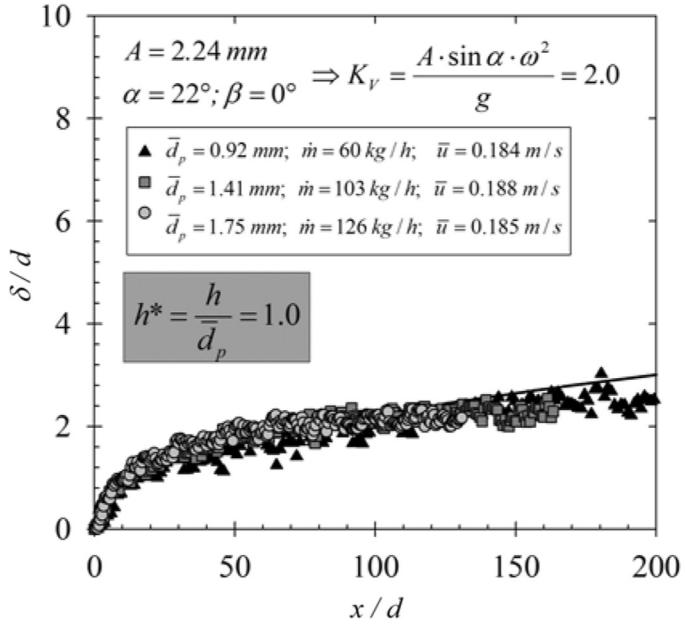


**Figure 13.** Growth of the mixing layer thickness for different size fractions and constant dimensionless bed height $h^* = 1.0$.

present DEM code. With the simulation of one certain case, i.e., to adjust the mass flow with a certain particle fraction in such a way that a dimensionless layer thickness of $h^* = 0.5$ is adapted, it is straightforward to check whether the experimental results can be reproduced.

Figure 14 shows the results of both the simulation and the experiments for a mean diameter of $\bar{d}_p = 0.92\,\text{mm}$. Although spherical particles were assumed in the simulation, good agreement between the measured and simulated results could be obtained.

The results of the simulation for a second case, i.e., with another particle size ($\bar{d}_p = 1.75\,\text{mm}$) but for the same constant dimensionless layer thickness, as seen in Figure 15, show that the DEM simulation also reproduces the experimentally observed effect that the mixing layer thickness collapses onto the same curve. This result proves that the present DEM code is able to simulate the dispersion on the vibrating conveyor qualitatively as well as quantitatively.

**Table 5.** Dispersion coefficients as fitted to the results of experiments presented in Figures 12 and 13

| Fraction/$\bar{d}_p$ [mm] | $D_y[m^2/s]$ for $h^* = 0.5$ | $D_y[m^2/s]$ for $h^* = 1.0$ |
|---|---|---|
| Small/0.92 | $0.90 \times 10^{-5}$ | $1.10 \times 10^{-6}$ |
| Medium/1.41 | $1.56 \times 10^{-5}$ | $1.74 \times 10^{-6}$ |
| Large/1.75 | $2.21 \times 10^{-5}$ | $2.13 \times 10^{-6}$ |

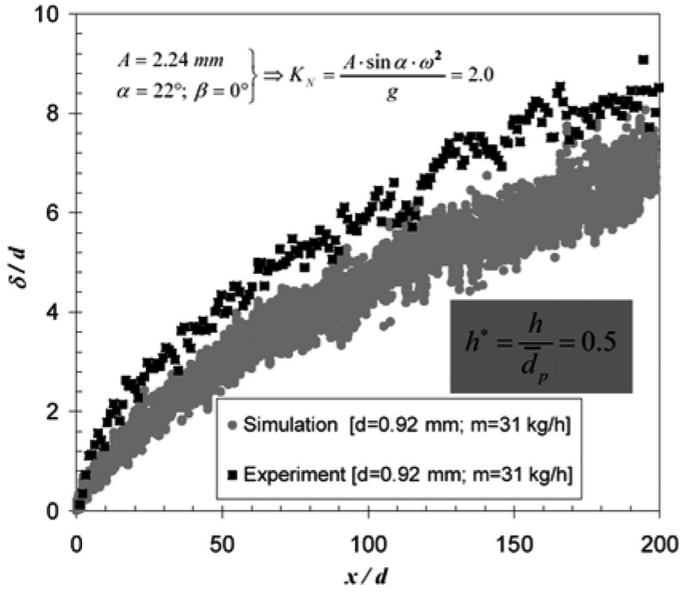


**Figure 14.** Comparison between simulated and measured results for $\bar{d}_p = 0.92\,\text{mm}$ and $\dot{m}_{in} = 31\,\text{kg/h}$.

The deviation between the simulated and measured results in Figure 15 and Table 6 was expected, since the simulations assume a spherical shape for the particles. However, in the experiments sand was used as granular material. Spherical

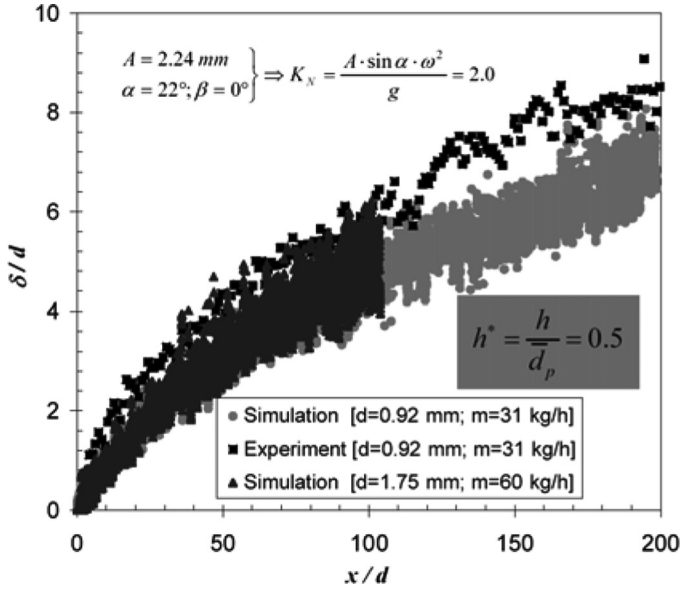


**Figure 15.** Comparison between simulated and measured results for $\bar{d}_p = 0.92\,\text{mm}$, $\dot{m}_{in} = 31\,\text{kg/h}$, $\bar{d}_p = 1.75\,\text{mm}$, $\dot{m}_{in} = 60\,\text{kg/h}$.

**Table 6.** Dispersion coefficients as extracted from experiments and numerical simulation

| Fraction/$\bar{d}_p$ [mm] | Experiment $D_y[m^2/s]$ for $h^* = 0.5$ | Simulation $D_y[m^2/s]$ for $h^* = 0.5$ |
|---|---|---|
| Small/0.92 | $0.90 \times 10^{-5}$ | $0.62 \times 10^{-5}$ |
| Large/1.75 | $2.21 \times 10^{-5}$ | $1.30 \times 10^{-5}$ |

particles move only through contacts among each other crossways to the vibrating conveyor; arbitrarily formed particles, in contrast, also move because of contacts with the trough in the cross direction. This and the fact that spherical particles roll much better than arbitrarily formed shapes probably lead to a reduced dimensionless layer thickness and dispersion coefficient in the simulations (see Figures 14 and 15 and Table 6).

## Conclusions

This article presents results of experimental and numerical investigations of the mixing behavior of thin granular layers on a vibrating conveyor. The mixing was found to be directly proportional to the vertical acceleration of the conveyor and indirectly proportional to the mass flow of the transported material. Keeping the above-mentioned parameters constant, the dispersion increased with increasing mean particle sizes. When performing the experiments with materials of different mean particle diameters and tuning the mass flow to achieve the same level of dimensionless bed height, the magnitude of the dispersion coefficient remained constant. Thus, the correctness of the utilization of the particle diameter in the dispersion equation is confirmed.

The numerical simulations of these cases showed good agreement between the measured and simulated results. Thereby the main factor for the differences is expected to result from the fact that the simulations are performed with spherical particles, whereas sand was used as granular material in the experiments. Hence, the ability and the quality of the present DEM code to simulate the dispersion on the vibrating conveyor are validated.

Decreasing the dimensionless bed height led to intensification of mixing, whereas increased bed height $h^* > 1$ drastically reduced the particle dispersion.

Increasing the height of the transported bed to a significant higher level $h^* >> 5$ by loading more material on the conveyor, which may enhance mixing again. As a consequence, the mechanisms responsible for the process are of totally different natures. The mixing occurs due to the convective displacement of particle lumps and depends strongly on the acceleration ratio $K_N$ (Hunt et al., 1994; Hsiau et al., 2002; Ko, 2005; Lu & Hsiau, 2005, Submitted; Tai & Hsiau, 2004; Akiyama & Nishiyama, 1994; Akiyama et al., 1998).

The observations described here may lead to some important conclusions explaining the behavior of the material submitted to vibration. Especially interesting is the transition between the single particle movement and the bulk transport regime. If the layer covering the trough is high enough, the free path among the single particles practically disappears and the material behaves as a collective. Then the dispersion within the bed may be neglected. For this case, the application of mathematical

models treating the transported material as a single block with complex physical properties seems to be a very robust and efficient tool to simulate the transport behavior of granular material (El hor & Linz, 2005). On the other hand, results of experiments carried out for small bed heights $h^* < 1$ are a very good tool to validate the applicability of DEM-based simulations, as shown in this study.

## References


Akiyama, T. & R. Nishiyama. 1994. Solid mixing in a vibrating particle bed: Effect of a tube submerged in the bed. *Powder Technol.* 80: 11–16.

Akiyama, T., T. Iguchi, K. Aoki, & K. Nishimoto. 1998. A fractal analysis of solids mixing in two-dimensional vibrating particle beds. *Powder Technol.* 97: 63–71.

Asmar, B. N., P. A. Langston, & A. J. Matchett. 2002. A generalized mixing index in distinct element method simulation of vibrated particulate beds. *Granular Matter* 4: 129–138.

Buggisch, H. & G. Löffelmann. 1989. Theoretical and experimental investigations into granulate mixing mechanisms. *Chem. Eng. Process.* 26: 193–200.

Campbell, C. S. 1990. Rapid granular flows. *Annu. Rev. Fluid Mech.* 22: 57–92.

Campbell, C. S. 1997. Self-diffusion in granular shear flows. *J. Fluid Mech.* 348: 85–101.

Cleary, P. W., G. Metcalfe, & K. Liffman. 1998. How well do discrete element granular flow models capture the essentials of mixing processes? *Appl. Math. Model.* 22: 995–1008.

Cundall, P. A. & O. D. L. Strack. 1979. A discrete numerical model for granular assemblies. *Geotechnique* 29 (1): 47–65.

Di Maio, F. P. & A. Di Renzo. 2004. Analytical solution for the problem of frictional-elastic collisions of spherical particles using the linear model. *Chem. Eng. Sci.* 59: 3461–3475.

El hor, H. & S. J. Linz. 2005. Model for transport of granular matter on annular vibratory conveyor. *J. Stat. Mech.* 2005: L02005.

Foerster, S. F., M. Y. Louge, H. Chang, & K. Allia. 1994. Measurements of the collision properties of small spheres. *Phys. Fluids* 6 (3): 1108–1115.

Goda, T. J. & F. Ebert. 2005. Three-dimensional discrete element simulations in hoppers and silos. *Powder Technol.* 158: 58–68.

Goetz, S. 2006. Gekoppelte CFD/DEM Simulation blasenbildenden Wirbelschichten. Ph.D. diss. University of Dortmund.

Grochowski, R. & P. Walzel. 2005. Dispersion of granular material on a vibrating conveyor. *Chem. Ing. Tech.* 77: 1020.

Grochowski, R., P. Walzel, M. Rouijaa, C. A. Krülle, & I. Rehberg. 2004a. Reversing granular flow on a vibratory conveyor. *Appl. Phys. Lett.* 84: 1019–1021.

Grochowski, R., S. Strugholtz, H. El hor, S. J. Linz, & P. Walzel. 2004b. Transport properties of granular matter on vibratory conveyors. Paper presented at International Congress for Particle Technology (PARTEC 2004), Nuremberg (16–18 March).

Henrique, C., G. Batrouni, & D. Bideau. 2000. Diffusion as a mixing mechanism in granular materials. *Phys. Rev. E* 63: 011304.

Hsiau, S. S. & M. L. Hunt. 1993. Shear-induced particle diffusion and longitudinal velocity fluctuations in a granular-flow mixing layer. *J. Fluid Mech.* 251: 299–313.

Hsiau, S. S. & S. C. Yang. 2003. Numerical simulation of self-diffusion and mixing in a vibrating granular bed with the cohesive effect of liquid bridges. *Chem. Eng. Sci.* 58: 339–351.

Hsiau, S. S., P. C. Wang, & C. H. Tai. 2002. Convection cells and segregation in a vibrated granular bed. *AIChE J.* 48: 1430–1438.

Hsiau, S. S., L. S. Lu, J. C. Chen, & W. L. Yang. 2005. Particle mixing in a sheared granular flow. *J. Multiph. Flow* 31: 793–808.

Hunt, M. L., S. S. Hsiau, & K. T. Hong. 1994. Particle mixing and volumetric expansion in a vibrated granular bed. *J. Fluids Eng.* 116: 785–791.

Ivanov, I., S. Wirtz, H.-J. Mühlen, & M. Mayer. 2004. Discrete Element Simulationen zur simultanen Beschreibung von Material- und Energietransport in bewegten Schüttungen. Paper presented at DGMK-Tagung Energetische Nutzung von Biomassen "Velen VI", Posterbeitrag, 19–21. April 2004.

Jenkins, J. T. & S. B. Savage. 1983. A theory for the rapid flow of identical, smooth, nearly elastic, spherical particles. *J. Fluid. Mech.* 130: 187–202.

Johnson, K. L. 1989. *Contact Mechanics*. Cambridge: Cambridge University Press.

Kharaz, A. H., D. A. Gorham, & A. D. Salman. 2001. An experimental study of the elastic rebound of spheres. *Powder Technol.* 120: 281–291.

Ko, Y. S. 2005. Vibrationsmischen von Schüttgütern bei stochastischer Anregung des Bechälters. Ph.D. diss. University of Paderborn.

Kruggel-Emden, H., E. Simsek, S. Wirtz, & V. Scherer. 2006a. Modeling of granular flow and combined heat transfer in hoppers by the discrete element method (DEM). *J. Press. Vessel Technol.* 128 (3): 439–444.

Kruggel-Emden, H., E. Simsek, S. Wirtz, & V. Scherer. 2006b. A new approach for modeling the normal contact within granular assemblies through the discrete element method. Paper presented at AIChE Fifth Congress on Particle Technology, Orlando.

Kruggel-Emden, H., E. Simsek, S. Wirtz, & V. Scherer. 2007. A comparative numerical study of particle mixing on different grate designs through the discrete element method. *J. Press. Vessel Technol.* 129: 4.

Kruggel-Emden, H., E. Simsek, S. Wirtz, & V. Scherer. 2007. Review and extension of normal force models for the discrete element method. *Powder Technol*. 171(3): 157–173.

Langston, P. A., M. A. Al-Awamleh, F. Y. Fraige, & B. N. Asmar. 2004. Distinct element modelling of non-spherical frictionless particle flow. *Chem. Eng. Sci.* 59: 425–435.

Lätzel, M., S. Luding, H. J. Herrmann, D. W. Howell, & R. P. Behringer. 2003. Comparing simulation and experiment of a 2D granular Couette shear device. *Eur. Phys. J. E* 11: 325–333.

Lu, L. S. & S. S. Hsiau. 2005. Mixing in vibrated granular beds with the effect of electrostatic force. *Powder Technol.* 160: 170–179.

Maw, N., J. R. Barber, & J. N. Fawcett. 1976. The oblique impact of elastic spheres. *Wear* 38: 101–114.

Natarajan, V. V. R., M. L. Hunt, & E. D. Taylor. 1995. Local measurements of velocity fluctuations and diffusion coefficients for a granular material flow. *J. Fluid Mech.* 304: 1–25.

Ogawa, S. 1978. Multi-temperature theory of granular materials. In *Proceedings of US-Japan Seminar on Continuum-Mechanical and Statistical Approaches in the Mechanics of Granular Materials, Tokyo* pp. 208–217.

Rhodes, M. J., X. S. Wang, M. Nguyen, P. Stewart, & K. Liffman. 2001. Study of mixing in gas-fluidized beds using a DEM model. *Chem. Eng. Sci.* 56: 2859–2866.

Rougier, E., A. Munjiza, & N. W. M. John. 2004. Numerical comparison of some explicit time integration schemes used in DEM, FEM/DEM and molecular dynamics. *Int. J. Numer. Meth. Eng.* 61: 856–879.

Schäfer, J., S. Dippel, & D. E. Wolf. 1996. Force schemes in simulations of granular materials. *J. Phys. I* (France) 6: 5.

Scott, A. M. & J. Bridgewater. 1976. Self-diffusion of spherical particles in a simple shear apparatus. *Powder Technol.* 14: 177–183.

Sommer, K. 1977. Mechanismen des Pulvermischens. *Chem. Ing. Tech.* 49: 305–311.

Tai, C. H. & S. S. Hsiau. 2004. Dynamic behaviors of powders in vibrated bed. *Powder Technol.* 139: 221–232.

Weinekötter, R. & H. Gericke. 2000. *Mixing of Solids*. Boston: Kluwer Academic.

Zik, O. & J. Stavans. 1991. Self-diffusion in granular flows. *Europhys. Lett.* 16: 255–258.